Charge density waves on a half-filled decorated honeycomb lattice

Chunhan Feng,[1,*] Huaiming Guo,[2] and Richard T. Scalettar[1]

[1]*Department of Physics, University of California, Davis, California 95616, USA*
[2]*Department of Physics, Key Laboratory of Micro-Nano Measurement-Manipulation and Physics (Ministry of Education),*
Beihang University, Beijing 100191, China

Tight binding models like the Hubbard Hamiltonian are most often explored in the context of uniform intersite hopping t. The electron-electron interactions, if sufficiently large compared to this translationally invariant t, can give rise to ordered magnetic phases and Mott insulator transitions, especially at commensurate filling. The more complex situation of nonuniform t has been studied within a number of situations, perhaps most prominently in multiband geometries where there is a natural distinction of hopping between orbitals of different degree of overlap. In this paper we explore related questions arising from the interplay of multiple kinetic energy scales and *electron-phonon* interactions. Specifically, we use determinant quantum Monte Carlo (DQMC) to solve the half-filled Holstein Hamiltonian on a "decorated honeycomb lattice," consisting of hexagons with internal hopping t coupled together by t'. This modulation of the hopping introduces a gap in the Dirac spectrum and affects the nature of the topological phases. We determine the range of t/t' values which support a charge density wave phase about the Dirac point of uniform hopping $t = t'$, as well as the critical transition temperature T_c. The QMC simulations are compared with the results of mean field theory.

I. INTRODUCTION

Itinerant electrons on a honeycomb lattice host a Dirac spectrum in the absence of interactions which has attracted considerable attention [1–6]. The linearly vanishing density of states (DOS) at $E = 0$ forms an interesting counterpoint to that of the square lattice (of interest to cuprate superconductivity) whose DOS diverges (logarithmically) at $E = 0$. An immediate consequence is that whereas in the square lattice, long-range antiferromagnetic (AF) correlations onset in the ground state for any finite repulsive interaction U, a nonzero critical U_c is required for AF order on the honeycomb lattice [7,8].

Recently, the effects of electron-phonon interactions on Dirac fermions have been explored [9,10]. Similar to the case of electron-electron interactions, the semimetallic band structure requires a critical electron-phonon interaction strength for charge density wave (CDW) formation at half filling. A crucial difference is that unlike Néel order which occurs only at $T = 0$ in the two-dimensional Hubbard model [11], owing to the continuous nature of the spin symmetry being broken, the CDW transition occurs at finite temperature.

In this paper we extend these investigations of the Holstein model on a honeycomb lattice by examining the effect of a regular pattern of nonuniform hopping. The particular "Kekulé hopping texture" we investigate has been proposed [12] to give rise to nontrivial topological properties associated with an opening of a gap at the Dirac point, and linked to the "pseudo-angular-momentum" of electrons residing on sets of strongly hybridized hexagons. Similar "decorated lattices"

have been studied previously in the context of the depleted square lattice Heisenberg [13] and Hubbard [14] Hamiltonians as possible theoretical descriptions of spin-liquid phases in CaV_4O_9 [15–19]. It was shown that while long-range antiferromagnetic correlations exist in the ground state when the hoppings t and t' are roughly balanced, spin-liquid phases consisting of independent spin dimers or spin plaquettes are present when the hoppings are sufficiently unequal. Within mean field theory, a rich variety of spin-ordered phases, characterized by different patterns of spin inside and between the plaquettes, can arise as a function of doping and U in such decorated Hubbard models [14].

Strongly correlated physics in the presence of several kinetic energy scales gives rise to a further variety of phenomena in other important realizations, including orbitally selective Mott transitions [20–26]. In the case of the periodic Anderson model, which includes both conduction c and local d orbitals, a dominant interorbital hopping $t_{cd} \gtrsim t_{cc}$ can lead to singlet formation and a spin-liquid ground state [27,28], as seen in quantum Monte Carlo studies in $d = 1, 2, 3$ and $d = \infty$ [29–32]. As in the less widely studied case of decoration, the existence of several hopping energy scales whose difference is large disrupts magnetic order. Most of these investigations have focused on electron-electron interactions.

We will discuss some interesting analogies between the spin-singlet formation in such situations and charge singlets in the electron-phonon case. However, it is important to emphasize that the Holstein model breaks the spin symmetry present in the Hubbard model, with charge order (the analog of ordering in the S^z channel) dominating over superconducting order (which maps onto S^x, S^y). As a result, the CDW transition in the half-filled 2D Holstein model occurs at finite temperature [33], whereas long-range magnetic order in the
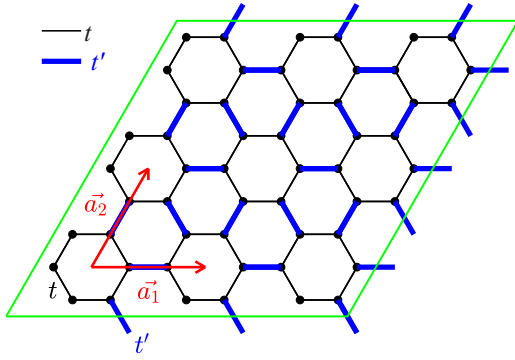
*chhfeng@ucdavis.edu

FIG. 1. The structure of the "decorated honeycomb lattice." Two different hopping strengths are present. Hybridization t (thin black lines) links the sites of a collection of independent hexagons. These hexagons are then connected by t' (thick blue lines). In the $t' \gg t$ limit, an alternate description in terms of elemental dimers linked by t is a more appropriate starting point.

2D Hubbard model occurs only at $T = 0$. This breaking of symmetry introduces a fundamental difference between the physics of the repulsive Hubbard and Holstein models with multiple hopping energy scales, which is especially marked as the phonon frequency ω_0 decreases.

This paper is organized as follows: Section II introduces the precise model we will investigate, along with our computational methodology. Section III discusses the results of mean field theory (MFT) calculations, which we show capture some of the tendency to reduced CDW order with nonuniform hoppings. Section IV contains the detailed determinant quantum Monte Carlo (DQMC) results and analysis, and is followed by some further discussion and interpretation in Sec. V.

II. MODEL AND METHODS

We investigate the Holstein Hamiltonian,

$$\hat{\mathcal{H}} = -\sum_{\langle \mathbf{ij} \rangle \sigma} t_{ij} \big(\hat{c}_{\mathbf{i}\sigma}^{\dagger} \hat{c}_{\mathbf{j}\sigma} + \hat{c}_{\mathbf{j}\sigma}^{\dagger} \hat{c}_{\mathbf{i}\sigma} \big) - \mu \sum_{\mathbf{i}\sigma} n_{\mathbf{i}\sigma}$$
$$+ \frac{1}{2} \sum_{\mathbf{i}} \hat{p}_{\mathbf{i}}^2 + \frac{1}{2} M \omega_0^2 \sum_{\mathbf{i}} \hat{x}_{\mathbf{i}}^2 + \lambda \sum_{\mathbf{i}} \hat{x}_{\mathbf{i}} (\hat{n}_{\mathbf{i}\uparrow} + \hat{n}_{\mathbf{i}\downarrow}). \quad (1)$$

Here the kinetic energy sum is over sites on a hexagonal lattice, with $t_{ij} = t$ for pairs of sites internal to a set of hexagons, and $t_{ij} = t'$ for pairs of sites bridging distinct hexagons. See Fig. 1. We will report lattice sizes N in terms of the number of hexagons, i.e., the unit cell count. Figure 1 corresponds to $N = (3 \times 3) \times 6 = 54$ sites. The remaining terms in $\hat{\mathcal{H}}$ consist of a collection of local quantum oscillators of frequency ω_0 ($\omega_0 = 1$ is used in all the simulations in this paper) and an electron-phonon coupling λ of the fermionic charge density $\hat{n}_{\mathbf{i}\uparrow} + \hat{n}_{\mathbf{i}\downarrow}$ to the displacement $\hat{x}_i$. We will measure the strength of the coupling via the dimensionless combination $\lambda_D \equiv \lambda^2/(M\omega_0^2 W)$. In the antiadiabatic limit $\omega_0 \to \infty$, the coupling λ_D can be thought of as the ratio of an effective attraction between electrons mediated by the phonons, $U_{\text{eff}} = -\lambda^2/(M\omega_0^2)$, to the kinetic energy scale W. The choice $t = 1 + \Delta$ and $t' = 1 - 2\Delta$ keeps the bandwidth $W = 6$ fixed as

Δ is varied, allowing us to study the effects of modulated hopping while keeping λ_D constant. We set the phonon mass $M = 1$ and tune the chemical potential $\mu = -\lambda^2/\omega_0^2$ to the particle-hole symmetry point so that the filling is always $\langle n_{\mathbf{i}\sigma} \rangle = \frac{1}{2}$.

We solve for the properties of Eq. (1) using two methods. The first is a mean field approach in which we make an ansatz for the phonon coordinates. (See Sec. III.) The resulting Hamiltonian is quadratic in the remaining fermion degrees of freedom and can be solved analytically. The free energy is minimized within the parameter space allowed in the ansatz. The second approach is DQMC [34,35]. Unlike MFT, it solves the many-body problem exactly, on finite lattices. DQMC has statistical errors associated with the sampling, which are on the order of 0.1% for local quantities like the double occupancy and energy, but can be several percent for global quantities like structure factors in the vicinity of phase transitions. DQMC also has "Trotter errors" [36–39] arising from the discretization of imaginary time. Because these Trotter errors are of the same order as, or smaller than, the statistical ones for the quantities we use in determining the phase boundary, we do not perform any extrapolation in the imaginary-time discretization. For all the work in this paper we use $\Delta\tau = 0.1$.

Regardless of the value of Δ, the decorated honeycomb lattice is bipartite, and hence the local fermionic pairs which form due to the effective attractive interaction U_{eff} mediated by the phonons tend to form a charge density wave phase at half filling. Previous investigations have determined the phase diagram in the λ_D-T plane for $t = t'$ [9,10]. For $\omega_0/t = 1$, there is a quantum critical point at $(\lambda_D)_c = 0.27$ above which CDW order forms in the ground state. T_c rises rapidly at $(\lambda_D)_c$, reaching a maximum value $T_c/t \sim 0.2$ at $\lambda_D \sim 0.5$. We are interested here in the effect of the nonuniform hoppings Δ on T_c and on $(\lambda_D)_c$. In the limits $\Delta = 0.5$ and $\Delta = -1$ the system separates into collections of independent hexagons and dimers, making long-range order impossible and $T_c = 0$ trivially.

The two-site unit cell of the honeycomb lattice is expanded by the decoration, so that now there are six bands. Figure 2 shows $E(\vec{k})$ for the undecorated honeycomb lattice $t = t'$ (central panel), the dimer limit $t < t'$ (top panel), and the hexagon limit $t' < t$ (bottom panel). In either case, the touching of the two bands at the Dirac cones which occurs at half filling and $t = t'$ is replaced by a gap.

The associated densities of states (DOSs) for the three cases are shown in Fig. 2 (right). Consistent with the dispersion relations of Fig. 2 (left), when $\Delta \neq 0$, the linearly vanishing DOS at $E = 0$ of the isotropic honeycomb lattice is replaced with a gap.

The decorated lattice geometry of Fig. 1 has been proposed as a generalization of the isotropic honeycomb lattice with a topological gap opened by the difference between the inter- and intra-plaquette hoppings [12]. The six resulting bands can be viewed as arising from the six single-electron states ("orbitals") which exist on each independent ($t' = 0$) hexagon and whose degenerate levels are broadened when $t' \neq 0$. The topological nature is not like that induced by spin-orbit coupling. Instead, it is similar to the 1D Su-Schrieffer-Heeger model, which also contains weak and strong bonds. Domain
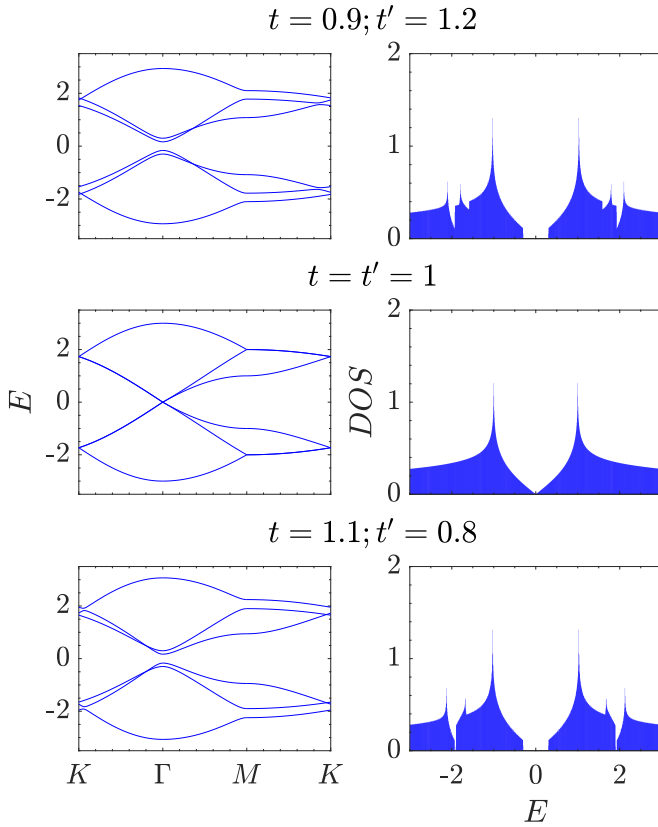
FIG. 2. Left: Energy dispersion $E(\vec{k})$ in the noninteracting ($\lambda = 0$) limit. The Dirac points of the two bands of the honeycomb lattice, $t = t'$ (middle panel), are split by the decoration $t \neq t'$. In both cases, $t > t'$ and $t < t'$, a gap is opened at half filling. See text for a discussion of differences at other fillings. Right: Density of states for the same three cases as left panel. A gap at half filling is evident when $t \neq t'$.
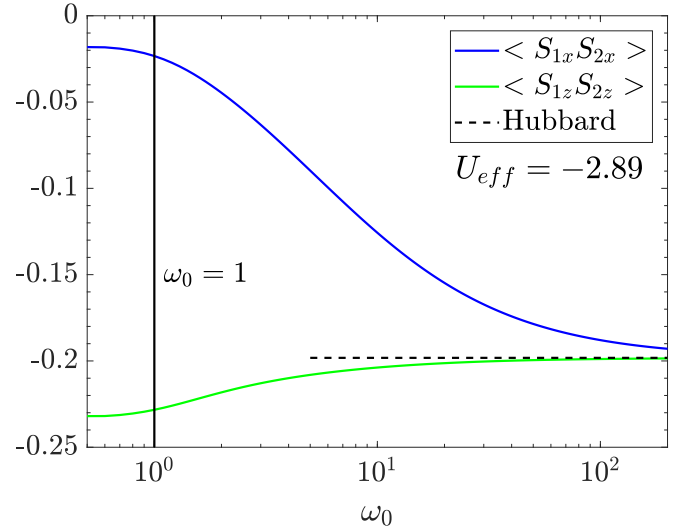

FIG. 3. Exact diagonalization results for the ground state charge, $\langle S_1^z S_2^z \rangle$, and superconducting, $\langle S_1^x S_2^x \rangle$, correlators (in magnetic language) on a two-site Holstein dimer, as a function of ω_0 at fixed $U_{\text{eff}} = -2.89$. The vertical line at $\omega_0 = 1$ shows the phonon frequency used in the phase diagram obtained in this paper. The dashed horizontal line is the Hubbard model result at $U = 2.89$. It is notable that values $\omega_0/t \lesssim 1$ are quite far from the limit where the spin correlations (CDW-pairing correlations) are symmetric.

walls which arise from $t \neq t'$ are associated with a gapless boundary state.

Other versions of decoration exist. For example, Rüegg *et al.* [40] have explored topological insulators of a tight-binding Hamiltonian with spin-orbit and Rashba interactions on a "star" lattice which interpolates between honeycomb and kagome geometries. Similarly, when honeycomb rhodates like Li_2RhO_3 are pressurized various bond dimerization patterns emerge on the Rh hexagons, and are associated with different magnetic patterns [41]. A final example is strained graphene, in which the hoppings t_1, t_2, t_3 along the three primitive lattice vectors are allowed to be unequal [42–45].

As noted in the introduction, in quantum spin-1/2 and itinerant electron Hamiltonians with repulsive interactions, unequal hoppings tend to degrade long-range magnetic order. It is worth discussing the relation between those (spin) singlet phases and the disordered phases in the attractive Hubbard model, since that has a close connection to the Holstein model studied here; both exhibit CDW and superconducting phases and a quantitative link is provided by $U_{\text{eff}} = -\lambda^2/\omega_0^2$.

In particular, consider the well-known particle-hole transformation (PHT) $c_{\mathbf{i}\downarrow}^\dagger \rightarrow (-1)^{\mathbf{i}} c_{\mathbf{i}\downarrow}$ on the down-spin fermions. On a bipartite lattice, and at $\mu = 0$, this PHT leaves the kinetic energy unchanged, but reverses the sign of the interaction

term. The different components of the spin operator map into charge and pairing correlations,

$$S_{\mathbf{i}}^z \equiv n_{\mathbf{i}\uparrow} - n_{\mathbf{i}\downarrow} \rightarrow n_{\mathbf{i}} \equiv n_{\mathbf{i}\uparrow} + n_{\mathbf{i}\downarrow},$$

$$S_{\mathbf{i}}^+ \equiv c_{\mathbf{i}\uparrow}^\dagger c_{\mathbf{i}\downarrow} \rightarrow \Delta_{\mathbf{i}}^\dagger \equiv (-1)^{\mathbf{i}} c_{\mathbf{i}\uparrow}^\dagger c_{\mathbf{i}\downarrow}^\dagger,$$

$$S_{\mathbf{i}}^- \equiv c_{\mathbf{i}\downarrow}^\dagger c_{\mathbf{i}\uparrow} \rightarrow \Delta_{\mathbf{i}} \equiv (-1)^{\mathbf{i}} c_{\mathbf{i}\downarrow} c_{\mathbf{i}\uparrow}. \quad (2)$$

This PHT yields insight into some of the expected physics in the presence of attractive interactions. In analogy with the formation of spin singlets in the repulsive case, for the attractive Hubbard and Holstein models we expect the development of "charge singlets" in which the three components of charge/pairing operators on the right side of Eq. (2) form local objects on either dimers or hexagons. These charge singlets might then compete with long-range CDW order when t and t' differ too greatly.

With this said, it is worth emphasizing that the Holstein ↔ Hubbard mapping is exact only in the antiadiabatic limit $\omega_0 \rightarrow \infty$. Figure 3 shows the effect of finite phonon frequency ω_0 on the different components of Eq. (2). Symmetry is restored as $\omega_0 \rightarrow \infty$, but for the value $\omega_0 = 1$ used in this paper, $|\langle S_1^z S_2^z \rangle| \gg |\langle S_1^x S_2^x \rangle|$. Thus, while the analogy to magnetic physics is useful, it is far from clear how it will manifest itself quantitatively. (The fact that these correlators are less in magnitude than the singlet value $-1/4$ is due to charge fluctuations. As U also becomes large, they approach the Heisenberg limit $-\frac{1}{4}$ so that $\vec{S}_1 \cdot \vec{S}_2 = -\frac{3}{4}$.)

III. MEAN FIELD RESULTS

We first examine the physics of the Hamiltonian of Eq. (1) within mean field theory. In this approach, we ignore the
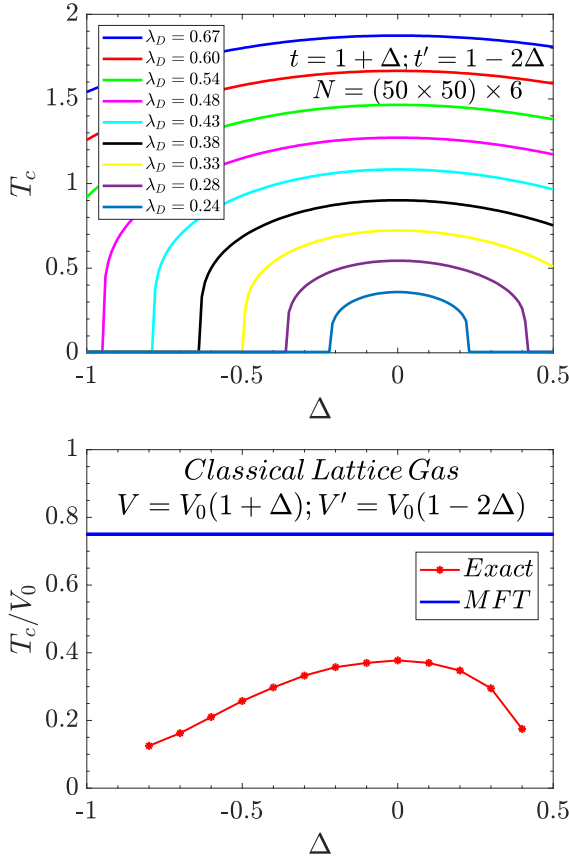
FIG. 4. Top: Dependence of T_c on λ_D of the decorated Holstein model Eq. (1) within mean field theory. The CDW transition temperature is maximized for isotropic hopping ($\Delta = 0$), and is suppressed on the dimer side $\Delta < 0$ and the hexagon side ($\Delta > 0$). Bottom: Comparison of T_c given by MFT and classical Monte Carlo for a classical lattice gas. The difference between exact T_c and MFT T_c is more significant when Δ approaches the limiting cases $\Delta = -1$ and $\Delta = 0.5$.

phonon kinetic energy and assume a staggered pattern for the phonon displacements, $x_i = x_0 + (-1)^i x_1$. Here $(-1)^i = \pm 1$ on the two sublattices of the (bipartite) honeycomb geometry. The quadratic fermion Hamiltonian can be diagonalized, resulting in a total free energy per site which combines both electron and phonon contributions, $f(x_0, x_1, T) = N \omega_0^2 (x_0^2 + x_1^2)/2 - T \sum_\alpha \ln(1 + e^{-\epsilon_\alpha(x_0,x_1)/T})$, where ϵ_α are the fermion energy levels. A nonzero bond dimerization x_1 implies an associated charge modulation, since λx_i acts as a local chemical potential on site i.

The resulting phase diagram is shown in the top panel of Fig. 4. T_c is decreased by decoration, as might be expected from the Stoner criterion and the opening of a true gap (vanishing of the Fermi surface density of states in a finite chemical potential range). However, for $\lambda_D = \frac{2}{3}$, the effect is relatively small: Even in the extreme independent hexagon and dimer limits, $T_c(\Delta = 0.5)/T_c(\Delta = 0) = 0.965$ and $T_c(\Delta = -1)/T_c(\Delta = 0) = 0.822$, respectively. The MFT T_c is nonzero even though there can be no symmetry breaking on small finite clusters. On the other hand, for smaller λ_D, MFT results indicate that a critical Δ is needed in order to have a CDW phase, which is consistent with the DQMC

results in Fig. 8. We have verified that for $\lambda_D > 0.24$, the MFT results shown for $(50 \times 50) \times 6$ lattices change by less than the thickness of the lines if the lattice size is decreased to $(4 \times 4) \times 6$, an observation which aids in interpreting the DQMC results of the next section, which are necessarily on smaller lattices. At $\lambda_D < 0.24$, where T_c becomes small and the CDW region is minute, finite-size effects, unsurprisingly, become more pronounced.

It is interesting to contrast this with the behavior of the simplest model of CDW physics in this geometry, the classical lattice gas $E = \sum_{\langle ij \rangle} V_{ij} n_i n_j$. Here $n_i = 0, 1$ and we choose $V_{ij} = V_0(1 + \Delta)$ or $V_{ij} = V_0(1 - 2\Delta)$, with the same geometry and bond convention as in Fig. 1. The total coupling $\sum_j V_{ij}$ at each site i is independent of Δ, in analogy to fixing the bandwidth W. The transition temperature as a function of Δ is given in the bottom panel of Fig. 4. Within MFT, T_c is completely independent of Δ because T_c is only a function of the total, and invariant, $\sum_j V_{ij}$. The bottom panel of Fig. 4 also gives the exact T_c (obtained by Binder crossings of classical Monte Carlo simulations). The exact T_c does depend on Δ, and can be seen to vary by a factor of 3 from its $\Delta = 0$ value when $\Delta = -0.8$ or $\Delta = +0.4$, values which approach the decoupled hexagon and dimer limits. Unlike the MFT calculation, the exact T_c must vanish at $\Delta = -1$ and $\Delta = +0.5$, and the lattice consists of independent clusters.

As we shall see in the following section, the MFT values for the critical temperature of Fig. 4 (top) are an order of magnitude larger than those of QMC. This is perhaps not too surprising given the low dimensionality being studied. We note that a similar comparison of phase diagrams for the 2D Hubbard model revealed MFT in considerable disagreement with DQMC [46].

IV. QUANTUM MONTE CARLO RESULTS

We now turn to the results of DQMC simulations which include fluctuations neglected in the preceding MFT treatment. We begin by showing the charge structure factor,

$$S_{cdw} = \frac{1}{N} \sum_{i,j} (-1)^{i+j} \langle n_i n_j \rangle, \tag{3}$$

with $(-1)^{i+j} = \pm 1$ according to whether sites i, j are on the same or different sublattices. In an ordered phase, $T < T_c$, we expect S_{cdw} to grow linearly with the lattice size since $\langle n_i n_j \rangle$ is nonzero even for widely separated i, j pairs.

Figure 5 gives S_{cdw} for several values of λ_D and lattice sizes N at low temperature, $\beta = 10$. In a window about the isotropic Holstein limit ($\Delta = 0$), S_{cdw} is large and increases with lattice size, suggesting the presence of long-range charge correlations for those values. Meanwhile, for large Δ, S_{cdw} is small and independent of size. Two quantum critical points (QCPs) Δ_c separate the CDW from charge singlet regions at the two extremes of hopping difference $\Delta = -1.0$ and $\Delta = 0.5$.

The difference

$$\mathcal{D} \equiv C_{nn} - C'_{nn} \equiv \langle n_i n_{i+\hat{x}} \rangle_t - \langle n_i n_{i+\hat{x}} \rangle_{t'} \tag{4}$$

between the near-neighbor density-density correlations C_{nn} on the t and t' bonds provides a measure of the effect of hopping
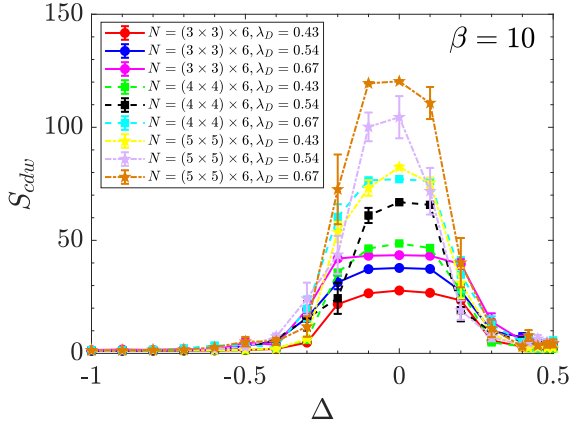
FIG. 5. Charge structure factor S_{cdw} as a function of hopping difference Δ. There is a window near the isotropic point $\Delta = 0$ in which S_{cdw} is large and scales with system size, indicating long-range charge order.

difference on the order. For Δ small, $\mathcal{D}$ is small. $\mathcal{D}$ rises rapidly in the vicinity of the QCPs Δ_c. See Fig. 6. Indeed, $d\mathcal{D}/d\Delta$ can be regarded as an "inhomogeneity susceptibility" which diverges at $T = 0$ as $\Delta \to \Delta_c$.

Figures 5 and 6 focus on the low-temperature charge correlations and identify the positions of the QCPs which bound the CDW regions near the isotropic lattice limit. Within the CDW, there is a finite-temperature phase transition as T is decreased. Crossings of the scaled structure factor $S_{cdw}/L^{\gamma/\nu}$ are shown in Fig. 7 and identify T_c in the region of small Δ where long-range order persists.

As discussed in the introduction, it seems natural to connect the loss of charge order in this electron-phonon model to analogous AF-singlet transitions in Hamiltonians describing quantum magnetism which have several exchange energy scales, e.g., the periodic Anderson and bilayer Hubbard Hamiltonians, and the bilayer or random bond Heisenberg Hamiltonians. We have used that language extensively in the present paper, since it does constitute a useful touchstone. However, the fact that a finite-temperature CDW transition occurs in the Holstein model suggests care should be taken in
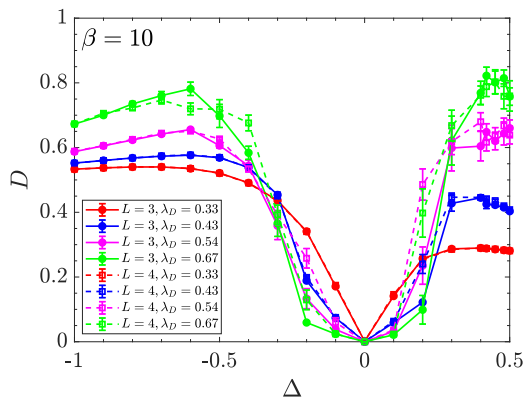

FIG. 6. Difference $\mathcal{D}$ between density correlation function on t and t' bonds as a function of Δ. $\mathcal{D}$ rises steeply in the vicinity of the CDW to charge singlet QCP.
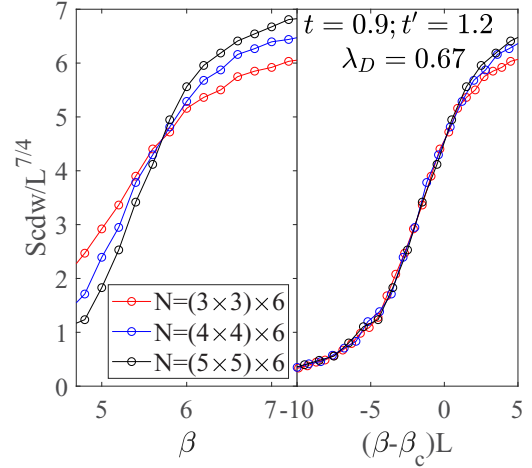

FIG. 7. Scaled structure factor $S_{cdw}/L^{\gamma/\nu}$ as a function of β. The scaling exponent $\gamma/\nu = 7/4$ is taken to be the 2D Ising value, and provides a good universal crossing. The crossing points identify $T_c = 1/\beta_c$.

emphasizing this connection, since the continuous symmetry of the ordering direction forbids such a finite-T transition in the 2D magnetic models. Indeed, Fig. 3 shows that the parameters explored in Figs. 5–7 are in fact very far from the regime where the analogy is precise.

Phase diagrams are obtained for fixed $\lambda_D = 0.48$, varying t and t' (top panel), and fixed $t = 0.9, t' = 1.2$, varying λ_D (bottom panel), in Fig. 8. It is numerically challenging to attempt to extract T_c when it becomes too small. Nevertheless, we can put reliable upper bounds on T_c by measuring S_{cdw} at large β and verifying that its value is consistent with only short-range charge correlations. Doing simulations at β up to $\beta = 25$ (temperature $T = 0.04$) strongly suggests that similarly to the undecorated honeycomb case [9,10], there is a nonzero critical coupling $(\lambda_D)_c \sim 0.32$, for $t = 0.9, t' = 1.2$, as indicated along the $T = 0$ axis in the bottom panel of Fig. 8. Correspondingly, for fixed $\lambda_D = 0.48$, large-β simulations suggest there are critical hopping differences Δ_c, as shown in the top panel of Fig. 8. The presence of these QCPs is further supported by their appearance in the MFT results in Fig. 4.

The fitting curves in Fig. 8 (top and bottom panels) are based on a simple cubic spline through the data and hence are best regarded as "guides to the eye." Since this is based on an *ad hoc* functional form, there is considerable uncertainty in the positions of the QCPs which are seen in the MFT treatment (Fig. 4).

We conclude by examining the single-particle spectral function, $A(\omega)$, which is related to the fermion Green's function $G(\tau)$ obtained in DQMC via

$$G(\tau) = \int d\omega \frac{e^{-\omega\tau}}{e^{\beta\omega} + 1} A(\omega). \tag{5}$$

$A(\omega)$ is the many-body analog of the single-particle density of states, and hence carries information concerning the opening of energy gaps in the excitation spectrum. We invert Eq. (5)
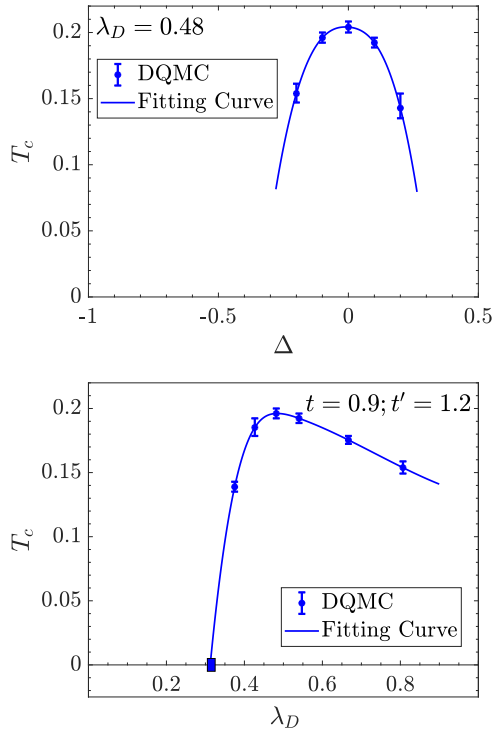
FIG. 8. Top: Phase diagram of T_c as a function of Δ when $\lambda_D = 0.48$. T_c reaches its maximum for isotropic hopping ($\Delta = 0$), and drops sharply on the dimer side $\Delta < 0$ and the hexagon side ($\Delta > 0$). Bottom: Phase diagram of T_c as a function of λ_D when $t = 0.9, t' = 1.2$ with $(\lambda_D)_c \sim 0.32$. As λ_D grows, T_c increases first, as the electron-phonon coupling induces the CDW phase, but then decreases as large values of the electron-phonon coupling cause the polarons to become increasingly heavy [9,10]. The symbol along the horizontal axis of the bottom panel is obtained by extrapolating the sharp descent of the DQMC data for T_c, combined with low-temperature simulations which show that the charge correlations are short ranged.

via the maximum-entropy method [47]. Figure 9 gives $A(\omega)$ for two values of hopping difference on opposite sides of the CDW–charge singlet QCP. Despite the difference in the nature of the ground state, $A(\omega)$ vanishes at the Fermi surface $\omega = 0$ in both cases, as T is lowered. In the case of larger Δ, this
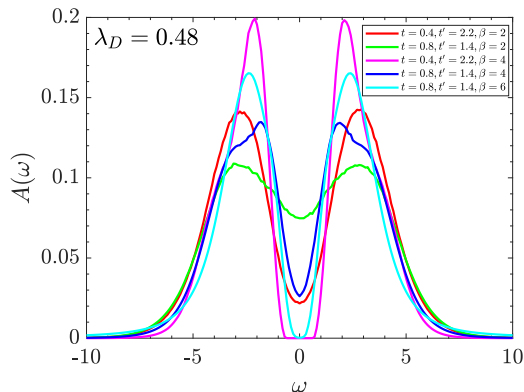

FIG. 9. Spectral function for the two cases $\Delta = -0.6$ in the charge liquid phase and $\Delta = -0.2$ in the CDW phase.

reflects the presence of a charge singlet gap. In the case of smaller Δ, this is a CDW gap. Similar behavior occurs on the two sides of the antiferromagnetic spin-singlet QCP in the multiband Hubbard model [48].

V. CONCLUSIONS

In this paper we have presented determinant quantum Monte Carlo results for the Holstein model with modulated hopping on a "decorated honeycomb lattice" which consists of a collection of weakly coupled hexagons or, in the opposite limit of the relative hybridizations, weakly coupled dimers. Our key result was the determination of the evolution of the charge density wave order as one moves away from uniform hopping toward either of these extremes. This work represents an extension of investigations of the competition between magnetically ordered and spin-liquid phases in decorated Hubbard Hamiltonians, to CDW–to–charge singlet transitions in electron-phonon models. The effect of $t_{x,y} = (1 \pm \Delta)$ on S_{cdw} has also been recently studied in the anisotropic square lattice Holstein Hamiltonian [49]. However, in this case the modulation end points $\Delta = -1, +1$ are decoupled, but still infinite, linear chains. In the present work the end points $\Delta = -1, +0.5$ result in small independent clusters. As a result of infinite clusters still being present, long-range order is somewhat more robust to modulation in the square lattice case.

The geometry we investigated has been proposed as a possible realization of a $\mathcal{Z}_2$ topological state associated with the "artificial orbitals" of the independent hexagons. As discussed in [12], it might be possible to implement this geometry via the placement of a triangular lattice of CO molecules on a Cu(111) surface. Our work has shown that in addition to topological properties, electron-phonon interactions can show a diverse set of charge-ordering behaviors on such lattices.

The strong breaking of the pairing-charge degeneracy distinguishes the present work from previous magnetic analogs. Specifically, what we demonstrate here is that despite the lack of "rotational" symmetry, local objects which have (imperfect) singlet character nevertheless still form on the strong bonds, and these ultimately lead to a loss of CDW order. This nontrivial result could not be anticipated by magnetic analogs where rotational symmetry is always exact. Indeed, we have provided a precise quantification of the Holstein-to-Hubbard mapping in the antiadiabatic limit. The data of Fig. 3 emphasize that the spin symmetry characterizing the Hubbard model is violated by more than a factor of 5 for the Holstein model at $\omega_0/t = 1$, by almost a factor of 2 at $\omega_0/t = 10$, and even at $\omega_0/t = 10^2$ a difference of 5% remains.

[1] F. D. M. Haldane, Model for a Quantum Hall Effect without Landau Levels: Condensed-Matter Realization of the "Parity Anomaly", Phys. Rev. Lett. **61**, 2015 (1988).

[2] C. L. Kane and E. J. Mele, Quantum Spin Hall Effect in Graphene, Phys. Rev. Lett. **95**, 226801 (2005).

[3] K. S. Novoselov, A. K. Geim, S. V. Morozov, D. Jiang, M. I. Katsnelson, I. V. Grigorieva, S. V. Dubonos, and A. A. Firsov, Two-dimensional gas of massless Dirac fermions in graphene, Nature (London) **438**, 197 (2005).

[4] G. Li and E. Y. Andrei, Observation of Landau levels of Dirac fermions in graphite, Nat. Phys. **3**, 623 (2007).

[5] B. Wunsch, F. Guinea, and F. Sols, Dirac-point engineering and topological phase transitions in honeycomb optical lattices, New J. Phys. **10**, 103027 (2008).

[6] T. O. Wehling, A. M. Black-Schaffer, and A. V. Balatsky, Dirac materials, Adv. Phys. **63**, 1 (2014).

[7] Thereza Paiva, R. T. Scalettar, W. Zheng, R. R. P. Singh, and J. Oitmaa, Ground state and finite temperature signatures of quantum criticality in the half-filled Hubbard model on a honeycomb lattice, Phys. Rev. B **72**, 085123 (2005).

[8] S. Sorella, Y. Otsuka, and S. Yunoki, Absence of a spin liquid phase in the Hubbard model on the honeycomb lattice, Sci. Rep. **2**, 992 (2012).

[9] Y.-X. Zhang, W.-T. Chiu, N. C. Costa, G. G. Batrouni, and R. T. Scalettar, Charge Order in the Holstein Model on a Honeycomb Lattice, Phys. Rev. Lett. **122**, 077602 (2019).

[10] Chuang Chen, Xiao Yan Xu, Zi Yang Meng, and Martin Hohenadler, Charge-Density-Wave Transitions of Dirac Fermions Coupled to Phonons, Phys. Rev. Lett. **122**, 077601 (2019).

[11] J. E. Hirsch and S. Tang, Antiferromagnetism in the Two-Dimensional Hubbard Model, Phys. Rev. Lett. **62**, 591 (1989).

[12] L.-H. Wu and Xiao Hu, Topological properties of electrons in honeycomb lattice with detuned hopping energy, Sci. Rep. **6**, 24347 (2016).

[13] M. Troyer, H. Kontani, and K. Ueda, Phase Diagram of Depleted Heisenberg Model for CaV_4O_9, Phys. Rev. Lett. **76**, 3822 (1996).

[14] E. Khatami, R. R. P. Singh, Warren E. Pickett, and Richard T. Scalettar, Magnetic Correlations and Pairing in the 1/5-Depleted Square Lattice Hubbard Model, Phys. Rev. Lett. **113**, 106402 (2014).

[15] S. Taniguchi, T. Nishikawa, Y. Yasui, Yukio Kobayashi, J. Takeda, S.-I. Shamoto, and M. Sato, Spin gap behavior of $S = 1/2$ quasi-two-dimensional system CaV_4O_9, J. Phys. Soc. Jpn. **64**, 2758 (1995).

[16] N. Katoh and M. Imada, Spin gap in two-dimensional Heisenberg model for CaV_4O_9, J. Phys. Soc. Jpn. **64**, 4105 (1995).

[17] K. Ueda, H. Kontani, M. Sigrist, and P. A. Lee, Plaquette Resonating-Valence-Bond Ground State of CaV_4O_9, Phys. Rev. Lett. **76**, 1932 (1996).

[18] M. P. Gelfand, Zheng Weihong, R. R. P. Singh, J. Oitmaa, and C. J. Hamer, Convergent Expansions for Properties of the Heisenberg Model for CaV_4O_9, Phys. Rev. Lett. **77**, 2794 (1996).

[19] W. E. Pickett, Impact of Structure on Magnetic Coupling in CaV_4O_9, Phys. Rev. Lett. **79**, 1746 (1997).

[20] A. Liebsch, Novel Mott Transitions in a Nonisotropic Two-Band Hubbard Model, Phys. Rev. Lett. **95**, 116402 (2005).

[21] R. Arita and K. Held, Orbital-selective Mott-Hubbard transition in the two-band Hubbard model, Phys. Rev. B **72**, 201102(R) (2005).

[22] K. Inaba and Akihisa Koga, Phase diagrams of the two-orbital Hubbard model with different bandwidths, Phys. Rev. B **73**, 155106 (2006).

[23] A. Koga, N. Kawakami, T. M. Rice, and M. Sigrist, Orbital-Selective Mott Transitions in the Degenerate Hubbard Model, Phys. Rev. Lett. **92**, 216402 (2004).

[24] M. Ferrero, F. Becca, M. Fabrizio, and M. Capone, Dynamical behavior across the Mott transition of two bands with different bandwidths, Phys. Rev. B **72**, 205126 (2005).

[25] L. de'Medici, A. Georges, and S. Biermann, Orbital-selective Mott transition in multiband systems: Slave-spin representation and dynamical mean-field theory, Phys. Rev. B **72**, 205124 (2005).

[26] S. Biermann, L. de'Medici, and A. Georges, Non-Fermi-Liquid Behavior and Double-Exchange Physics in Orbital-Selective Mott Systems, Phys. Rev. Lett. **95**, 206401 (2005).

[27] P. A. Lee, T. M. Rice, J. W. Serene, L. J. Sham, and J. W. Wilkins, Theories of heavy-electron systems, Commun. Condens. Mater. Phys. **12**, 99 (1986).

[28] T. Nishino and Kazuo Ueda, Spin- and charge-excitation gaps in the one-dimensional periodic Anderson model, Phys. Rev. B **47**, 12451 (1993).

[29] R. M. Fye, Quantum Monte Carlo study of the one-dimensional symmetric Anderson lattice, Phys. Rev. B **41**, 2490 (1990).

[30] M. Jarrell, Hossein Akhlaghpour, and Th. Pruschke, Periodic Anderson Model in Infinite Dimensions, Phys. Rev. Lett. **70**, 1670 (1993).

[31] M. Vekić, J. W. Cannon, D. J. Scalapino, R. T. Scalettar, and R. L. Sugar, Competition between Antiferromagnetic Order and Spin-Liquid Behavior in the Two-Dimensional Periodic Anderson Model at Half Filling, Phys. Rev. Lett. **74**, 2367 (1995).

[32] C. Huscroft, A. K. McMahan, and R. T. Scalettar, Magnetic and Thermodynamic Properties of the Three-Dimensional Periodic Anderson Hamiltonian, Phys. Rev. Lett. **82**, 2342 (1999).

[33] M. Weber and Martin Hohenadler, Two-dimensional Holstein-Hubbard model: Critical temperature, Ising universality, and bipolaron liquid, Phys. Rev. B **98**, 085405 (2018).

[34] R. Blankenbecler, D. J. Scalapino, and R. L. Sugar, Monte Carlo calculations of coupled boson-fermion systems. I, Phys. Rev. D **24**, 2278 (1981).

[35] S. R. White, D. J. Scalapino, R. L. Sugar, E. Y. Loh, Jr., J. E. Gubernatis, and R. T. Scalettar, A numerical study of the two-dimensional Hubbard model with repulsive Coulomb interaction, Phys. Rev. B **40**, 506 (1989).

[36] H. F. Trotter, On the product of semi-groups of operators, Proc. Am. Math. Soc. **10**, 545 (1959).

[37] M. Suzuki, Generalized Trotter's formula and systematic approximants of exponential operators and inner derivations with applications to many-body problems, Commun. Math. Phys. **51**, 183 (1976).

[38] R. M. Fye, New results on Trotter-like approximations, Phys. Rev. B **33**, 6271 (1986).

[39] R. M. Fye and R. T. Scalettar, Calculating specific heats and susceptibilities using the Trotter approximation, Phys. Rev. B **36**, 3833 (1987).

[40] A. Rüegg, Jun Wen, and Gregory A. Fiete, Topological insulators on the decorated honeycomb lattice, Phys. Rev. B **81**, 205115 (2010).

[41] V. Hermann, S. Biswas, J. Ebad-Allah, F. Freund, A. Jesche, A. A. Tsirlin, M. Hanfland, D. Khomskii, P. Gegenwart, R. Valentí, and C. A. Kuntscher, Pressure-induced formation of rhodium zigzag chains in the honeycomb rhodate Li_2RhO_3, Phys. Rev. B **100**, 064105 (2019).

[42] Anand Sharma, Valeri N. Kotov, and Antonio H. Castro Neto, Interacting Anisotropic Dirac fermions in strained graphene and related systems, arXiv:1206.5427.

[43] S. Sorella, Kazuhiro Seki, Oleg O. Brovko, T. Shirakawa, Shohei Miyakoshi, Seiji Yunoki, and Erio Tosatti, Correlation-Driven Dimerization and Topological Gap Opening in Isotropically Strained Graphene, Phys. Rev. Lett. **121**, 066402 (2018).

[44] O. V. Gamayun, V. P. Ostroukh, N. Gnezdilov, I. Adagideli, and C. W. J. Beenakker, Valley-momentum locking in a graphene superlattice with Y-shaped Kekulé bond texture, New J. Phys. **20**, 023016 (2018).

[45] Elias Andrade, Ramon Carrillo-Bastos, and Gerardo G. Naumis, Valley engineering by strain in Kekulé-distorted graphene, Phys. Rev. B **99**, 035411 (2019).

[46] J. E. Hirsch, Two-dimensional Hubbard model: Numerical simulation study, Phys. Rev. B **31**, 4403 (1985).

[47] J. E. Gubernatis, Mark Jarrell, R. N. Silver, and D. S. Sivia, Quantum Monte Carlo simulations and maximum entropy: Dynamics from imaginary-time data, Phys. Rev. B **44**, 6011 (1991).

[48] A. Euverte, S. Chiesa, R. T. Scalettar, and G. G. Batrouni, Magnetic transition in a correlated band insulator, Phys. Rev. B **87**, 125141 (2013).

[49] B. Cohen-Stead, N. C. Costa, E. Khatami, and R. T. Scalettar, Effect of strain on charge density wave order in the Holstein model, Phys. Rev. B **100**, 045125 (2019).